Stability Control of an Hybrid Wheel-Legged Robot

G. Besseron, Ch. Grand, F. Ben Amar, F. Plumet, and Ph. Bidaud

Laboratoire de Robotique de Paris (LRP)
CNRS FRE 2507 - Université Pierre et Marie Curie, Paris 6
18 route du Panorama - BP61 - 92265 Fontenay-aux-Roses, FRANCE
{besseron,grand,amar,plumet,bidaud}@robot.jussieu.fr

Abstract

For exploration missions with autonomous robotic systems, one of the most important goal of any control system is to ensure the vehicle integrity. In this paper, the control scheme of an hybrid wheel-legged robot is presented. This scheme uses artificial potential field for the on-line stability control of the vehicle. First, the principle of this method is outlined and, then, simulation results in 2-D are presented.

Keywords: Control, stability, potential field, hybrid wheel-legged robot.

1 Introduction

The general field of this research is the mobility of autonomous robots navigating over an unknown natural environment like those come accross during exploration missions.

Autonomous exploration missions, like planetary and volcanic exploration or various missions in hazardous areas or sites under construction, require mobile robots that can move on a wide variety of terrains while insuring the system integrity.

One of the main difficulties in this kind of environment is due to the geometrical and physical soil properties (large slopes, roughness, rocks distribution, soil compaction, friction characteristics, etc). Hybrid robots (like Gofor [1], SRR [2], Workpartner [3] robots), which combine both the advantages of wheeled and legged robotic systems, are new locomotion systems specially designed to overcome these difficulties. They are

articulated vehicles with active internal mobilities which can be used to improve the stability.

HyLoS I [4] and HyLoS II, which have been designed and built at the LRP, are other examples of high mobility redundantly actuated (16 degrees-of-freedom) hybrid robots.

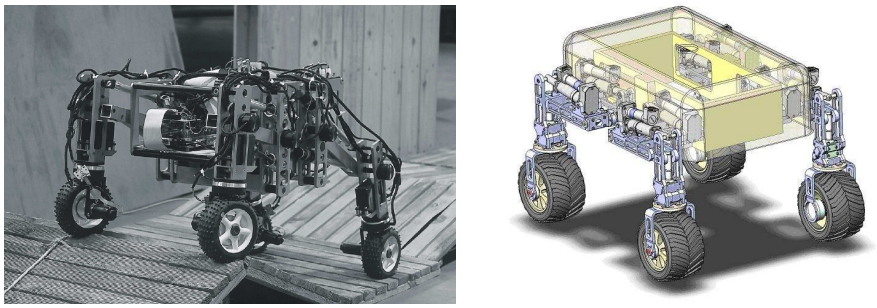

(a) HyLoS I (b) HyLoS II (CAD View)

Fig. 1. Hybrid Robots of LRP

Both systems have the ability to adapt their configuration and locomotion modes to the local difficulties of the crossed terrain. Previous published works have focused on the kinematic-based decoupling control of HyLoS [5] as well as on the comparison of locomotion performance [6].

However, uses of the internal mobilities to guarantee the robot integrity (i.e. stability) at all time is clearly inefficient from the energy consumption point of view.

In this paper, a new control scheme derived from the potential field approach is proposed. The scheme takes advantage of the capability of this method to merge different operational constraints and of the zero-band of the used potential fonctions.

In the next three sections, the kinematic model of the robot and the control scheme will be outlined. In the last section, simulation results of this control law will be shown and discussed.

2 Kinematic Model of HyLoS II

The kinematic of Hylos II is similar to HyLoS I one [4]. The main difference in HyLoS II (**Fig.** 1(b)) is the internal passive revolute joint linking the left and right part of the robot. Each part is composed of two articulated legs, which are made up of two degrees-of-freedom suspension mechanism and a steering and driven wheel. The control strategy is based on the velocity model of the vehicle. On the assumption that the rolling is ideal, Grand [5] proposes a velocity model of the system HyLoS I. The same formalism is used and adapted to the specific kinematic of HyLoS II, leading to $\mathbf{L}\dot{\mathbf{x}} + \mathbf{J}\dot{\boldsymbol{\theta}} = \mathbf{0}$ which can also be written as:

$$\begin{bmatrix} \mathbf{L} \, \mathbf{J} \end{bmatrix} \begin{bmatrix} \dot{\mathbf{x}} \\ \dot{\boldsymbol{\theta}} \end{bmatrix} = 0 \qquad \text{or} \qquad \mathbf{H}\,\dot{\mathbf{q}} = \mathbf{0} \tag{1}$$

where $\mathbf{L}$ is the Locomotion matrix which gives wheel contribution to plateform movement, $\mathbf{J}$ corresponds to the Jacobian matrix of wheel-legged kinematic chain, and $\mathbf{q}^T = [\mathbf{x}^T, \boldsymbol{\theta}^T]$ is the vector of robot parameters where $\mathbf{x}$ and $\boldsymbol{\theta}$ are respectively vectors of plateform parameters and articular-joint parameters of each wheel-legged subsystem.

Then virtual potential forces $\mathbf{F_i}$, described in the next section, are used to control the $\dot{\mathbf{q}}$ in the vehicle space configuration by considering the kinematic constraints of the system.

3 Proposed Approach

The main idea of this approach consists in using a driving virtual force $\mathbf{F_i}$ parallel to the opposite gradient of some potential field U_i.

$$\mathbf{F_i} = -\boldsymbol{\nabla} U_i \tag{2}$$

Khatib [7] was the first to describe this approach, which has been extensively used over the last two decades. This method is quite flexible since it can include other operational and functional constraints. The total potential field U can result from numerous functions U_i defined by:

$$U = \sum \alpha_i U_i(\mathbf{q}) \tag{3}$$

where U_i express potential function for obstacle avoidance, path tracking [8], joint limit avoidance or, in the present case, to guarantee the stability of the system. An influence coefficient α_i is allocated to each potential function to give more or less importance to the considered potential function.

3.1 Stability Constraint

Navigation on rough terrain requires to define a stability margin index. The "tipover stability margin" proposed by Papadopoulos in [9] is used.

This tipover stability margin takes into account both the distance of the projected center-of-gravity (CoG) to the support polygon and its vertical position relatively to the average plane defined by contact points P_i. Moreover, all the external forces including gravity are considered to work on the CoG of the vehicle. The formalism can be described briefly as follows (**Fig.** 2(a)) : the line joining two consecutive terrain-contact points P_i defines a tipover axis. The unit vector $\mathbf{l_i}$ of the axis joining the vehicle CoG, G, to the center of each tipover axis is computed. Then, the angle υ_i between each $\mathbf{l_i}$ and the total external force $\tau_\mathbf{t}$ applied to the vehicle gives the stability angle over the corresponding tipover axis.

Considering only quasi-static evolution of the vehicle here, the total external force $\tau_\mathbf{t}$ is reduced to its own weight. The stability margin m_{s_i} is therefore defined as the angle between $\mathbf{l_i}$ and the gravity resultant $\mathbf{g}$.

However, contrary to the original tipover stability margin, which uses the overall vehicle stability margin (defined as the minimum of all stability angles), one stability margin m_{s_i} per tumbling axis is defined in order to get a differential form for the potential field.

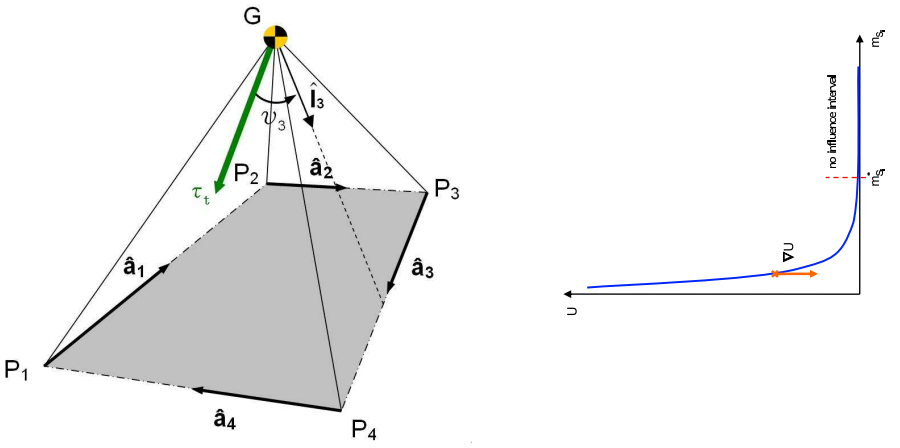

(a) (b)

Fig. 2. Stability Margin and associated Potential Function

So as to control the stability of the vehicle, a potential function is associated with each tipover axis and is defined by :

$$U_i = \begin{cases} \frac{1}{2}\,\xi\left(\frac{1}{m_{s_i}} - \frac{1}{m^*_{s_i}}\right)^2 & \text{if} \quad m_{s_i} \leq m^*_{s_i} \\ 0 & \text{if} \quad m_{s_i} > m^*_{s_i} \end{cases} \tag{4}$$

where m_{s_i} is the computed stability margin corresponding to each tumbling axis, $m^*_{s_i}$ is a stability margin limit, and ξ is a constant gain. This function has a zero-band (**Fig.** 2(b)), that results in the robot control of having a correction only is necessary. That is more efficient to the control from the energy consumption point of view.

3.2 Overall Control Scheme

The overall control scheme is shown in **Fig. 3**.

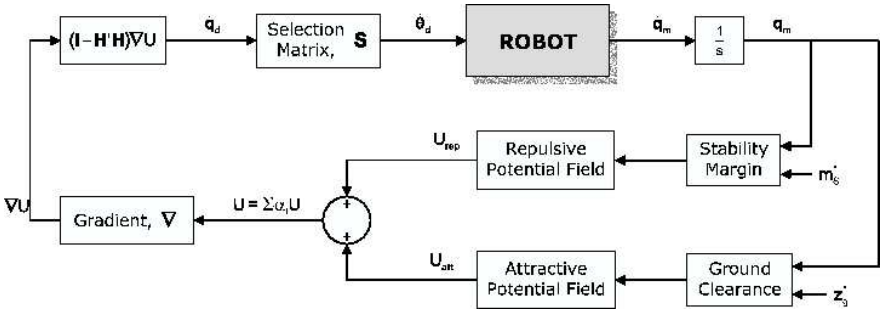

Fig. 3. Synoptic Control Scheme of robot

The control loop applied to the robot consists in moving away from a stability margin limit $m^*_{s_i}$ (defined in section 3.1) and, in the same time, in keeping the ground clearance – height of plateform – near the nominal value z^*_g. As defined in section 3.1, this control used potential functions associated to each criterion. The movement of the robot is not given here by any potential function but the angular speed of the wheels is forced. Therefore, a repulsive potential function relative to the stability margin $U_{rep_{sm}}$ and an attractive potential function to the ground clearance $U_{att_{gc}}$ are computed in this control loop.

The command set point **u** is then computed to follow the opposite gradian function of the required potential field projected on a constraints surface:

$$\mathbf{u} = -\mathbf{S}(\mathbf{I} - \mathbf{H}^{+}\mathbf{H})\boldsymbol{\nabla} U \tag{5}$$

where $\mathbf{H}^{+}\mathbf{H}$ refers to term of projection on surface of kinematic contraints in contact, U is the total potential field developed previously and $\mathbf{S}$ is a selection matrix.

4 Results

The proposed strategy is validated in 2-D simulation. This assumption could be explained by the kinematic of the robot, briefly presented in section 2. This 2-D consideration leads to the calculation of two stability margins (one per leg) m_{s_1} and m_{s_2} – in 2-D, there are only two tipover axis.

The validation of the stability control has been made on a terrain, which has a lot of slopes higher and higher (**Fig. 4**). A simulation in open loop (without reconfiguration) and another in feedback loop have been computed on this terrain.

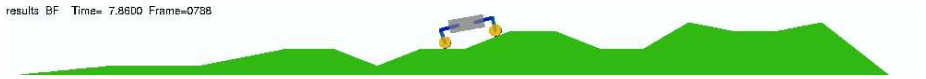

Fig. 4. Terrain of Simulation

The results of this simulation show the overall stability margin M_s comparison between open loop and feedback loop behaviour – this overall stability margin is defined as the minimum of all stability angles: $M_s = min(m_{s_i})$. Unlike open loop behaviour of robot, in feedback loop, the stability margin is constrained to move away from a stability margin limit that is ensured by associated potential function (Eq. 4). Each time the stability margin m_{s_i} gets closer to the stability margin limit $m^*_{s_i}$, the robot configuration is modified to move away from it. Thus, at the start of the simulation (**Fig.** 5(a): Time $<$ 6 sec) when the slopes are not too high (**Fig. 4**), the potential field has no influence on the robot configuration.

Compared with open loop behaviour, the overrun of stability margin limit is very small in feedback loop (**Fig.** 5(a)): the vehicle integrity in closed loop control is ensured.

Concerning the results of ground clearance measurement (**Fig.** 5(b)), as for stability, there is no correction by the associated potential function

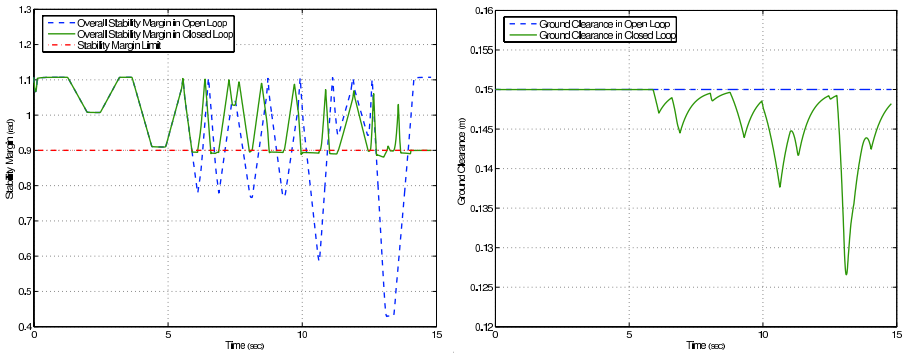

(a) Stability Margin (b) Ground Clearance

Fig. 5. Simulation Results

at the beginning of the simulation. The ground clearance is evaluated as the mean height of the robot legs, that is the reason why it is constant in open loop control. In feedback loop, the robot control attempts to bring ground clearance back to z_g^*. The results show than more sloping the terrain is, higher is the overrun of initial ground clearance z_g^*. This can be explain by the more important reconfiguration of the robot on high slopes, what involves one higher disturbance on ground clearance and a greater difficulty not to go over the stability margin limit $m_{s_i}^*$. The used control is a combination between two opposite actions, a compromise between the two defined potential functions – one which attempts to lift down the robot plateform and the other which lifts it up.

5 Conclusion

An original method to control the stability of a robotic system was proposed in this paper. This method gives interesting first results. Nevertheless some parameters of control must be sharpened. An extended simulation to 3D is planned in order to take into account the overall robot behaviour. Another interesting side, which could be evaluated, is the expected gain of energy consumption with this control strategy. Lastly, an experiment campaign will be hold with HyLoS II plateform.

References

1. Sreenivasan, S.V. and Wilcox, B.H. (1994) Stability and traction control of an actively actued micro-rover. *Journal of Robotics Systems*, vol. 11, no. 6, pp. 487–502.
2. Iagnemma, K., Rzepniewski, A., Dubowsky, S., and Schenker, P. (2003) Control of robotic vehicles with actively articulated suspensions in rough terrain. *Autonomous Robots*, vol. 14, no. 1, pp. 5–16.
3. Halme, A., Leppänen, I., Salmi, S., and Ylönen, S. (2000) Hybrid locomotion of a wheel-legged machine. In *3rd Int. Conference on Climbing and Walking Robots (CLAWAR'00)*.
4. BenAmar, F., Budanov, V., Bidaud, P., Plumet, F., and Andrade, G. (2000) A high mobility redundantly actuated mini-rover for self adaptation to terrain characteristics. In *3rd Int. Conference on Climbing and Walking Robots (CLAWAR'00)*, pp. 105–112.
5. Grand, C., BenAmar, F., Plumet, F., and Bidaud, P. (Oct. 2004) Stability and traction optimisation of a reconfigurable wheel-legged robot. *Int. Journal of Robotics Research*, vol. 23, no. 10-11, pp. 1041–1058.
6. Besseron, G., Grand, Ch., BenAmar, F., Plumet, F., and Bidaud, Ph. (2004) Locomotion modes of an hybrid wheel-legged robot. In *7th Int. Conf. on Climbing and Walking Robots*, Madrid, Spain.
7. Khatib, O. (1986) Real-time obstacle avoidance for manipulators and mobile robots. *Int. Journal of Robotics Research*, vol. 5, no. 1.
8. rensen, M.J. Sø Artificial potential field approach to path tracking for a non-holonomic mobile robot. .
9. Papadopoulos, E.G. and Rey, D.A. (1996) A new mesure of tipover stability for mobile manipulators. In *IEEE Int. Conf. on Robotics and Automation, ICRA'96*, pp. 3111–3116.